Theoretical Study of Thermal Decomposition Mechanisms of Isoxazole

James Higgins, Xuefeng Zhou, and Ruifeng Liu*

Department of Chemistry, East Tennessee State University, Johnson City, Tennessee 37614-0695

Received: March 18, 1997; In Final Form: June 4, 1997[⊗]

Density functional theory and ab initio calculations were carried out to investigate two probable unimolecular decomposition channels of isoxazole. The calculated structural parameters, dipole moment, and vibrational frequencies of isoxazole are in good agreement with available experimental data. Relative energies of transition states and equilibrium structures evaluated at MP4 and QCISD(T) levels of theory at B3LYP/6-31G** structures indicate that CO and CH_3CN, major products of isoxazole thermal decomposition in the temperature range 850−1100 K, are unlikely produced via the mechanism proposed in the experimental and previous theoretical studies. Instead, the mechanism proposed in the current study, isoxazole → $NCCH_2CHO$ → CH_3CN + CO, is more likely the main unimolecular decomposition channel. The mechanism proposed in the experimental study was shown to have a higher activation barrier and is likely responsible for the formation of HCN and H_2CCO, minor products of isoxazole decomposition.

I. Introduction

Isoxazole and its derivatives are important structural units of many molecules of biological interests.[1] Due to this reason, they have been the subject of extensive experimental studies.[2] Recently, thermal decomposition of isoxazole was studied[3] behind reflected shocks in a pressurized-driver single-pulse shock tube over the temperature range 850−1100 K. Acetonitrile and carbon monoxide were found to be the major products followed by hydrogen cyanide, propionitrile, and acetylene. Formation of carbon monoxide and hydrogen cyanide was suggested[3,4] to be via unimolecular processes and to follow the mechanism described in Scheme 1. According to this scheme, the reaction leading to acetonitrile and carbon monoxide proceeds via a hydrogen shift from position 5 to position 4, coupled by concerted N−O and C_4−C_5 bond cleavage, hydrogen shift from position 3 to position 4, and removal of carbon monoxide from the ring. The formation of hydrogen cyanide was suggested to follow a very similar process, but after the hydrogen shift from position 5 to position 4, C_4−C_3 instead of C_5−C_4 bond cleavages coupled with N−O bond rupture to give hydrogen cyanide and ketene. There are, however, some problems with the proposed mechanism. First, experiments[3] performed in a large quantities of toluene as a radical scavenger found that there is no effect on the production of acetonitrile but a small effect on the formation of hydrogen cyanide. Second, a very recent ab initio study[4] at the Hartree−Fock/3-21G level failed to find the transition structure (**TS2** of Scheme 1) of the major product channel leading to acetonitrile and carbon monoxide. Transition state searches located a transition structure for HCN + H_2CCO → CH_3CN + CO instead. However, on the basis of intrinsic reaction coordinate (IRC) and classical trajectory calculations, it was concluded[4] that the major products were formed by bifurcation due to a dynamical effect in the course of thermal decomposition.

Although we do not dispute that dynamical effects may play important roles in a chemical reaction, the above explanation is not completely convincing. This is because the ab initio study[4] found that according to Scheme 1, the transition state leading to the formation of HCN and $H_2C{=}C{=}O$ has a much lower activation energy, but HCN and $H_2C{=}C{=}O$ were observed only as minor products. Furthermore, if the formation of CH_3CN and CO follows a similar mechanism as the formation of HCN and $H_2C{=}C{=}O$, why does the radical scavenger not have any effect on the formation of the former but has a small effect on the latter? In our opinion, it may be evidence for different mechanisms being responsible for the formation of CH_3CN + CO and HCN + $H_2C{=}C{=}O$. A conceivable mechanism is described in Scheme 2. This mechanism does not involve a radical intermediate. Therefore, if the reaction follows this mechanism, a radical scavenger will have no effect on it.

SCHEME 1: Mechanism of Isoxazole Decomposition Proposed in Ref 3

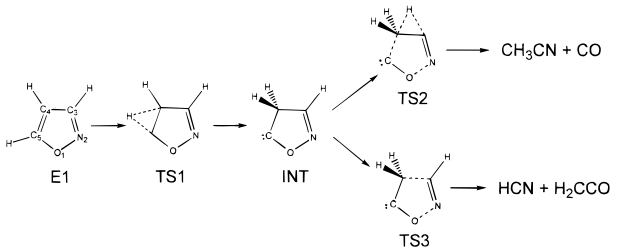

SCHEME 2: Mechanism of Isoxazole Decomposition Proposed in the Present Study

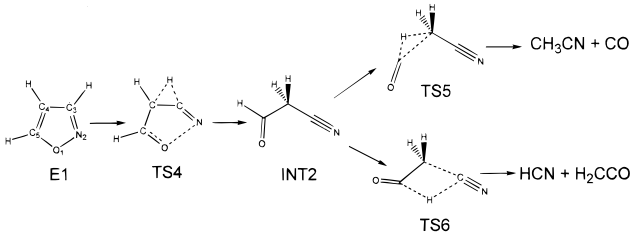

To reconcile the experimental and theoretical results and gain a better understanding this reaction, we have performed a detailed quantum mechanical study of the reaction channels described in Schemes 1 and 2.

II. Computational Details

All calculations were carried out using Gaussian94 program package.[5] The equilibrium and transition state structures were

[⊗] Abstract published in *Advance ACS Abstracts,* August 1, 1997.

S1089-5639(97)00976-6 CCC: $14.00

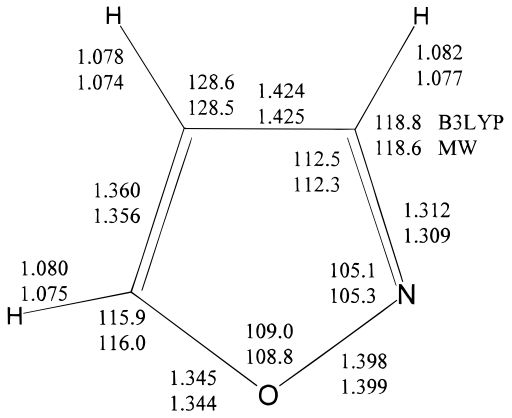

Figure 1. Calculated and experimental structural parameters of isoxazole (bond length in angstroms and angles in degrees).

fully optimized by Becke's three-parameter hybrid DFT/HF method[6] using the Lee−Yang−Parr correlation functional[7] (B3LYP) and the 6-31G** basis set.[8] Vibrational analyses were carried out, at the same level of theory, to characterize the optimized structures as equilibrium or transition states. Intrinsic reaction coordinate (IRC) analyses were performed on the transition structures to make sure the transition states connect the desired reactants and products. Energies of the optimized structures were evaluated at the B3LYP/6-31G** structures by B3LYP/6-311++G**, MP4(SDQ)(FC)/6-31G**, and MP4(SDTQ)(FC)/6-311++G**. For some critical structures, single-point energy calculations were also carried out at the QCISD(T)/6-311++G** level to obtained more reliable activation energies. Zero-point vibrational energies (ZPE) were taken into account and were approximated by one-half of the sum of B3LYP/6-31G** harmonic frequencies. The B3LYP/6-31G** harmonic frequencies were also used to evaluate activation enthalpies and activation entropies which were required for evaluating rate constants of the proposed decomposition channels by transition-state theory.

III. Results and Discussions

3.1. Structure, Dipole Moment, and Vibrations of Isoxazole. The calculated B3LYP/6-31G** structural parameters of isoxazole are compared with microwave structural parameters[9] in Figure 1. In the figure, bond lengths are given in angstroms and angles in degrees. It is shown that the calculated structural parameters are in excellent agreement with the experimental results. The largest difference between the calculated and microwave bond lengths is 0.004 Å. The largest difference between the calculated and microwave bond angles is 0.4°. At the equilibrium structure, the dipole moment calculated by B3LYP/6-31G** is 2.96 D. Experimentally, the dipole moment obtained from dielectric constant measurements[10] in benzene is 2.76 and 2.83 D. The result obtained from dielectric constant measurement[11] in dioxane is 3.01 D. The result obtained from microwave spectrum[12] is 2.90 D. These results indicate that B3LYP/6-31G** reproduces both the structural parameters and dipole moment of isoxazole accurately.

At the B3LYP/6-31G** equilibrium structure isoxazole, harmonic vibrational frequencies were calculated from B3LYP/6-31G** force constants evaluated as the second derivatives of energy. It has been well-known[13] that for most organic molecules, B3LYP/6-31G* harmonic frequencies are slightly higher than the corresponding fundamental frequencies. However, the difference between B3LYP/6-31G* harmonic and fundamental frequencies is quite systematic; therefore, a detailed scaling of B3LYP harmonic frequencies reproduces observed fundamental frequencies closely.[13,14] The scale factor derived[13] from minimizing the difference between the calculated and observed frequencies of many organic molecules is 0.963. We have applied this scale factor to the B3LYP/6-31G** harmonic frequencies of isoxazole and compared the results with experimental assignments[15] of fundamental vibrational modes in Table 1. Infrared intensities of the vibrational modes calculated from B3LYP/6-31G** dipole moment derivatives are also presented in this table. Mode descriptions given in this table are based on total vibrational energy distribution analysis.[16] Table 1 shows that for frequencies below 800 cm^{-1} and higher than 1300 cm^{-1}, the calculated and experimental frequencies are in good agreement. The mean deviation is 14.6 cm^{-1}, which is mainly contributed by C−H stretching modes. If the CH stretching modes are excluded, the mean deviation is less than 8 cm^{-1}. However, the difference between the calculated and observed frequencies in the range 800−1300 cm^{-1} is significantly larger. Careful inspection of the calculated and observed results indicates that the large differences are most likely due to misassignments of three vibrational modes in the experimental studies. The calculations indicate that vibrational modes ν_{12} and ν_{15} have very low infrared intensities (0.01 and 1.15 km/mol, respectively). Our HF/6-31G** calculations indicate that they also have very low Raman activities (0.91 and 0.45 $Å^4$/amu, respectively). Thus they are not expected easily seen in either an IR or Raman spectrum. Experimentally, a band at 792 cm^{-1} was assigned to ν_{15}, and a band at 916 cm^{-1} was assigned to ν_{12}. The former is 45 cm^{-1} lower than the calculated frequency of ν_{15} and is not close to any of the calculated frequencies. The latter is 31 cm^{-1} higher than the calculated frequency of ν_{12} but is only 18 cm^{-1} higher than the calculated frequency of ν_{11}. In fact, the experimental assignments of ν_8 (1217 cm^{-1}), ν_9 (1128 cm^{-1}), ν_{10} (1091 cm^{-1}), ν_{11} (1026 cm^{-1}), and ν_{12} (916 cm^{-1}) are very close to the calculated frequencies of ν_7 (1209 cm^{-1}), ν_8 (1118 cm^{-1}), ν_9 (1090 cm^{-1}), ν_{10} (1013 cm^{-1}), and ν_{11} (898 cm^{-1}), respectively. The experimental assignment of ν_7 to 1260 cm^{-1} is more than 50 cm^{-1} away from the calculated frequencies. These results indicate that the infrared and Raman bands observed at 1260 and 792 cm^{-1} are probably not due to fundamental vibrational modes of isoxazole,

TABLE 1: Calculated and Observed Vibrational Frequencies of Isoxazole

		calc[a]		obs[b]	assign[c]	
sym	ν	freq	I_{IR}[d]	freq	freq	mode description[e]
a′	1	3178	0.89	3161	3161	CH str
	2	3156	0.01	3131	3131	CH str
	3	3134	1.98	3089	3089	CH str
	4	1555	8.59	1557	1557	C═N and C═C str
	5	1422	31.04	1429	1429	C═C and C═N str
	6	1360	5.62	1366	1366	CH bend and ring def
	7	1209	6.21	1260	1217	CH bend
	8	1118	18.95	1217	1128	CO and CC str + CH bend
	9	1090	7.94	1128	1091	CC and CO str + CH bend
	10	1013	5.26	1091	1026	CC str + CH bend
	11	898	10.39	1026	916	ring def
	12	885	1.15	916		ring def
	13	855	25.65	845	845	NO str
a″	14	874	4.21	891	891	CH wag
	15	837	0.01	792		CH wag
	16	757	45.48	765	765	CH wag
	17	622	2.76	632	632	ring tor
	18	584	12.49	595	595	ring tor

[a] B3LYP/6-31G** harmonic frequencies scaled by 0.963. [b] Assignment of fundamental vibrational frequencies of ref 15. [c] Assignment of observed frequencies based on the calculated results. [d] B3LYP/6-31G** IR intensities in km/mol. [e] Based on total vibrational energy distribution analysis.

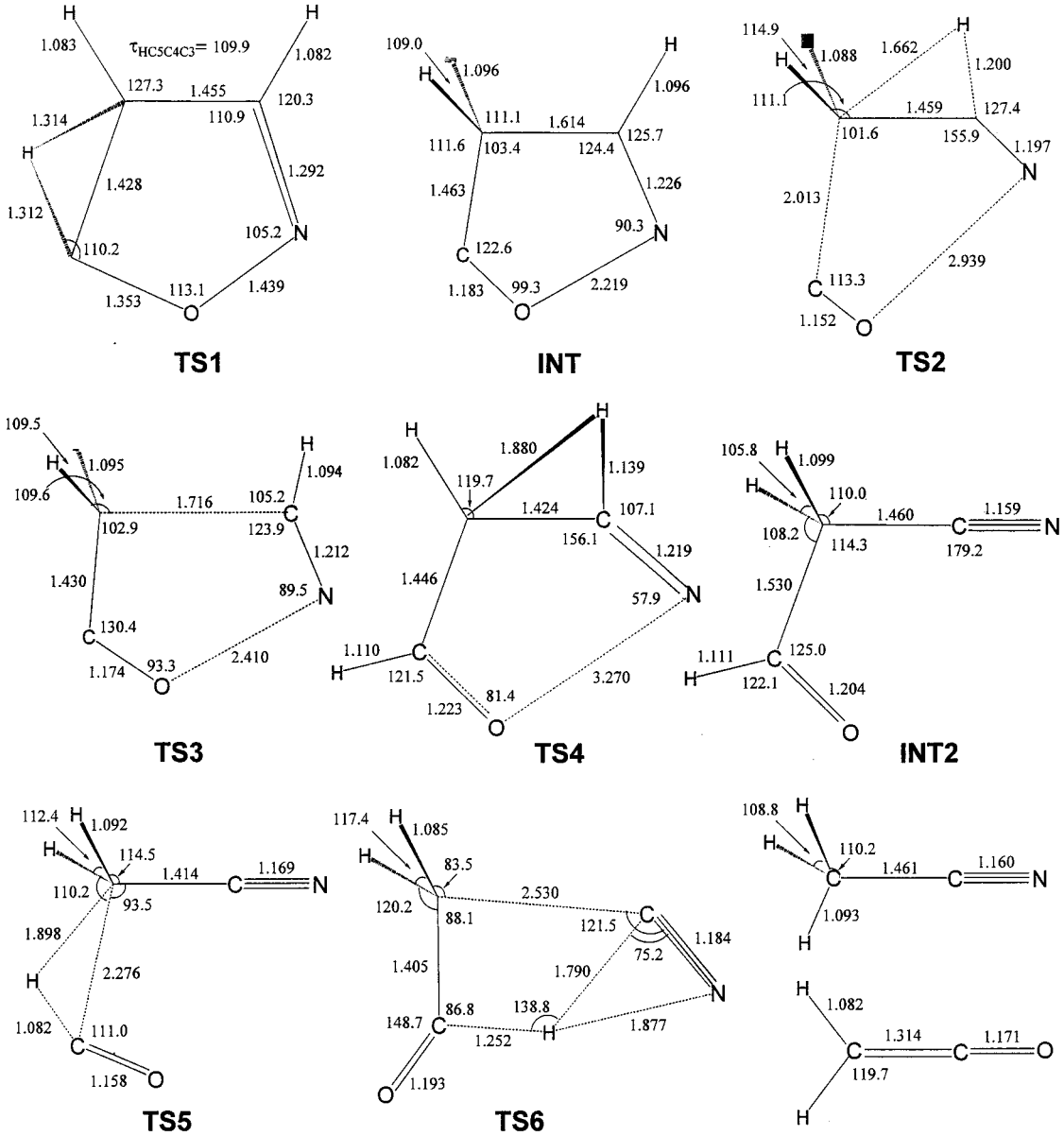

Figure 2. B3LYP/6-31G** structural parameters (bond length in angstroms and angles in degrees) of the transition states and equilibrium structures of isoxazole decomposition along Schemes 1 and 2.

and the experimental assignments of modes $\nu_8-\nu_{12}$ should be shifted up one place. The band at 1260 cm^{-1} was observed to be weak in both infrared and Raman spectra, and it was found to have a polarization ratio of 0.1 in the Raman spectrum. It is likely due to an overtone of ν_{17} (2×632 $cm^{-1} = 1264$ cm^{-1}). On the basis of the calculated results, reassignments of the fundamental frequencies of isoxazole are given in Table 1. This reassignment leaves ν_{12} and ν_{15} unassigned. According to the reassignments, mean deviation between the calculated and observed frequencies of isoxazole is 13 cm^{-1}, which is consistent with the mean deviation between the calculated and fundamental frequencies of many other organic compounds.

3.2. Structures and Energies of Critical Points along the Decomposition Channels. The B3LYP/6-31G** structural parameters of the transition states and intermediates of the decomposition channels depicted in Schemes 1 and 2 are presented in Figure 2. All the transition structures were checked for connecting the desired reactants and products by B3LYP/6-31G** IRC analyses. For Scheme 1, a significant difference between our B3LYP results and the Hartree−Fock results of Okada and Saito[4] is found with the transition structure **TS2**. The Hartree−Fock study of Okada and Saito failed to locate a transition state for **INT** → CH_3CN + CO. They found a transition structure similar to **TS2**, but their Hartree−Fock IRC analysis indicates that the structure is a transition state for HCN + H_2CCO → CH_3CN + CO. Contrary to their results, our B3LYP/6-31G** IRC analysis indicates that **TS2** we located is indeed the transition state for **INT** → CH_3CN + CO. The difference must be due to neglecting electron correlation by the HF method.

Along Scheme 2, the first transition state, **TS4,** has a very long O−N distance (3.270 Å). The long O−N bond makes the reaction step look like a stepwise process (O−N cleavage followed by hydrogen migration), but our B3LYP/6-31G** IRC analysis indicates that **TS4** is the only transition state for N−O cleavage and hydrogen migration from C_3 to C_4. The activation entropy for the reaction to produce CH_3CN + CO derived from analyzing experimental data is small, implying a tight transition state. **TS4** is, however, a quite loose transition state. The discrepancy might be explained by the fact that **INT2** is quite low in energy. Due to collisional deactivation, **TS5** may also play important roles in CH_3CN + CO formation.

From the B3LYP/6-31G** structural parameters, **TS6** looks like a transition state for **INT2** → HCN + H_2CCO. However,

TABLE 2: Energies[a] of Critical Structures of Isoxazole Decomposition along Schemes 1 and 2[b]

	E1	TS1	INT	TS2	TS3	TS4	INT2	TS5	TS6	$CH_3CN + CO$	$HCN + H_2CCO$
						6-31G**					
B3LYP	−246.039 63	72.9	43.5	70.4	43.7	64.9	−15.9	57.2	108.2	−18.2	8.17
MP2	−245.336 42	76.4	32.1	69.4	35.1	77.9	−21.4	57.4	120.7	−28.3	5.0
MP4(SDQ)	−245.356 09	72.3	45.2	69.3	45.4	73.3	−24.8	58.1	114.8	−34.3	1.9
						6-311++G**					
B3LYP	−246.103 94	72.3	39.4	64.1	38.6	59.1	−20.6	50.1	99.5	−25.7	−1.1
MP2	−245.436 46	74.4	27.2	61.1	28.7	71.5	−24.8	49.3	110.1	−32.9	−1.1
MP4(SQD)	−245.452 93	72.1	41.1	62.1	40.6	67.8	−28.1	50.9	104.5	−39.2	−3.9
MP4(SDTQ)	−245.496 92	71.2	28.6	55.4	29.2	63.7	−25.2	47.6	103.6	−36.0	−2.1
QCISD	−245.453 88	71.8				62.9				−38.4	−3.4
QCISD(T)	−245.491 15	70.9				58.5				−34.8	−1.0
ZPE[c]	36.4	32.6	33.2	29.8	32.4	30.8	34.5	31.2	27.9	31.7	30.2

[a] Total energy of **E1** is given in hartrees. The energies of the other structures are given in kcal/mol relative to **E1**. [b] The structures are given in Figures 1 and 2 as well as in Schemes 1 and 2. [c] Zero-point vibrational energy (in kcal/mol) approximated by one-half of the B3LYP/6-31G** harmonic vibrational frequencies.

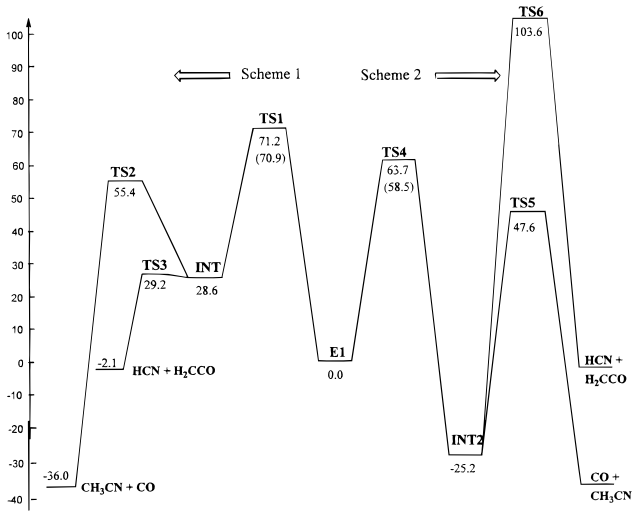

Figure 3. Schematic MP4(SDTQ)/6-311++G** potential energy profiles of isoxazole decomposition along Schemes 1 and 2. The numbers in parentheses are results of more expensive QCISD(T)/6-311++G** calculations.

our B3LYP/6-31G** IRC analysis indicates that the products are CNH + H_2CCO instead of HCN + H_2CCO. Our B3LYP/6-31G** calculations indicate that the isomerization of CNH to HCN has an activation barrier of 29.9 kcal/mol at B3LYP/6-31G** plus ZPE level. Results in Table 2 show that **TS6** is about 100 kcal/mol higher in energy than isoxazole, indicating that if the reaction proceeds via **TS6**, there would be enough excess energy in the CNH fragment so that the CNH produced can easily isomerize to the more stable form HCN. Since there are lower energy pathways, the decomposition from **INT2** → **TS6** → CNH + H_2CCO is unlikely to occur (see discussion below).

Relative energies of the critical structures along the reaction channels described in Schemes 1 and 2 are evaluated at the B3LYP/6-31G** structures by B3LYP/6-311++G**, MP4(SDQ)/6-31G**, and MP4(SDTQ)/6-311++G**. The results are presented in Table 2. Relative energies calculated by MP4(SDTQ)/6-311++G** are also presented schematically in Figure 3. It is shown that along Scheme 1, the highest energy barrier occurs at **TS1**, which is about 70 kcal/mol higher than isoxazole. The intermediate **INT,** which is produced via **TS1**, is only 0.6 kcal/mol lower than **TS3** at the MP4(SDTQ)/6-311++G** level. When ZPE is taken into consideration, **TS3** becomes lower in energy than **INT**, indicating **TS3** disappears when the zero-point vibrational energy is considered. Therefore the production of HCN and H_2CCO from isoxazole along Scheme 1 appears to go through a concerted hydrogen shift from C_5 to C_4, coupled with C_4-C_3 and O−N bond cleavage. On the other hand, **TS2** has been confirmed by B3LYP/6-31G** IRC analysis to be a transition state connecting **INT** and CO + CH_3CN. Thus the molecule overcoming the energy barrier at **TS1** may roll down in two directions. One will roll down hill all the way to produce HCN + H_2CCO. The other will roll down first and then climb another hill peaked at **TS2** and then roll down from there to produce CO + CH_3CN. Since the production of HCN + H_2CCO does not require the molecules to go over another barrier after **TS1**, HCN, and H_2CCO must be the favored products along Scheme 1.

Along Scheme 2, the first barrier occurs at **TS4**, which is about 10 kcal/mol lower than **TS1** at the highest level of theory applied. A very stable intermediate **INT2** is produced via **TS4**. This intermediate can decompose either via **TS5** to produce CO + CH_3CN or via **TS6** to produce HCN + H_2CCO. Since **TS6** is much higher in energy than all other transition states, it represents the least probable reaction path. Therefore the favorable decomposition channel along Scheme 2 is via **TS4** and **TS5** to produce CO + CH_3CN. As both **TS4** and **TS5** are lower in energy than **TS1**, CO and CH_3CN are predicted to be produced through Scheme 2 and are the major products, while HCN and H_2CCO are produced through Scheme 1. Since there is no radical intermediate involved in Scheme 2, radical scavenger should have no effect on the production of CO and CH_3CN, a fact in agreement with experimental result.[3]

Assuming the overall rate of a reaction channel is determined by the step of highest activation energy, it appears that the most important transition states for the two decomposition channels are **TS1** and **TS4**, respectively. To get a more reliable estimate of the activation energies of the two decomposition channels, we carried out more expensive QCISD(T)/6-311++G** energy calculations at **E1**, **TS1**, and **TS4**. The activation energies of **TS1** and **TS4** estimated from the QCISD(T) energies plus ZPE correction are 67.1 and 52.9 kcal/mol, respectively. The activation energy for CH_3CN production derived from fitting experimental data to the Arrhenius equation is 44 kcal/mol[3]. The difference between the calculated and experimental activation energies is 9 kcal/mol.

3.3. Transition State Theory Calculation of Rate Constants. To understand the difference between the calculated and experimental activation energies, we evaluated rate constants, by transition-state theory, of the two decomposition channels by assuming that **TS1** and **TS4** are the corresponding rate-determining transition structures. According to transition-state theory,[17] the rate constant k is given by the following formula:

TABLE 3: Rate Constants of Isoxazole Decomposition Calculated by Transition-State Theory

temp, K		850	900	950	1000	1050	1100
TS1	$\Delta H^{\ddagger}$ (kcal/mol)[a]	67.2	67.2	67.1	67.1	67.1	67.0
	$\Delta S^{\ddagger}$ (cal/mol K)[b]	−0.189	−0.235	−0.281	−0.327	−0.372	−0.418
TS4	$\Delta H^{\ddagger}$ (kcal/mol)[a]	54.9	54.9	54.8	54.8	54.8	54.7
	$\Delta S^{\ddagger}$ (cal/mol K)[b]	8.615	8.577	8.536	8.493	8.449	8.404
k_1 (s^{-1})		8.5×10^{-5}	8.0×10^{-4}	6.3×10^{-3}	3.8×10^{-2}	2.0×10^{-1}	9.0×10^{-1}
k_4 (s^{-1})		10	65	3.6×10^{2}	1.6×10^{3}	6.0×10^{3}	2.1×10^{4}
k_{co}(exptl)[c] (s^{-1})		4.2	18	65.6	210	604	1575

[a] Calculated from QCISD(T)/6-311++G** electronic energies and B3LYP/6-31G** vibrational frequencies. [b] Calculated from B3LYP/6-31G** vibrational frequencies. [c] Calculated from Arrhenius formula with the experimental preexponential factor and activation energy reported in ref 3.

$$k = \left(\frac{k_B T}{h}\right) e^{\Delta S^{\ddagger}/R} e^{\Delta H^{\ddagger}/RT}$$

where k_B is Boltzmann's constant, h is Planck's constant, $\Delta S^{\ddagger}$ is the activation entropy, and $\Delta H^{\ddagger}$ is the activation enthalpy. The thermodynamical parameters, $\Delta S^{\ddagger}$ and $\Delta H^{\ddagger}$, were evaluated by statistical thermodynamics from the calculated electronic energies and vibrational frequencies of the reactants and transition states. On the basis of QCISD(T)/6-311++G**//B3LYP/6-31G** energies and the B3LYP/6-31G** force fields, the calculated thermodynamical parameters of **E1**, **TS1**, and **TS4** at temperatures from 850 to 1100 K are given in Table 3. Rate constants calculated by the above equation are also given in this table. To compare with experimental results, we calculated rate constants for CO production from the preexponential factor and activation energy derived from experiments.[3] Table 3 shows that in the temperature range of the experimental study, the rate constants calculated from transition state theory are about 3−10 times larger than the rate constants calculated from the experimental preexponential factor and activation energy. Two factors might contribute to the difference between the calculated and "experimental" rate constants. First, the transition-state theory is a very crude model for estimating rate constants of a chemical reaction. Second, under the experimental conditions, many **INT2** molecules will lose most of their thermal energies by collisional deactivation. Those that lose their excess thermal energies will need additional energy to decompose to CH_3CN + CO. Taking into account of these factors, the agreement between the calculated and "experimental" rate constants appears reasonable.

IV. Conclusions

Density functional theory and high-level ab initio quantum mechanical calculations were carried out to investigate two probable unimolecular decomposition channels of isoxazole. The experimental structural parameters, dipole moment, and vibrational frequencies were reproduced accurately by density functional theory B3LYP/6-31G** method. Relative energies calculated by MP4 and QCISD(T) at transition structures optimized by B3LYP/6-31G** indicate that the production of CO + CH_3CN and the production of HCN + H_2CCO proceed via two different mechanisms with the former having a lower activation barrier. On the basis of the calculated results, we propose that CO and CH_3CN, major products of isoxazole thermal decomposition, are produced via the channel: isoxazole → $NCCH_2CHO$ → CO + CH_3CN. This is contrary to the conclusions of the experimental and previous lower level theoretical studies. The proposed mechanism may also be operative for unimolecular decomposition of the isoelectronic molecules furane and pyrrole and therefore may represent a unimolecular decomposition pattern of five-membered heterocyclic aromatic compounds.

Acknowledgment. This study was partially supported by the Research and Development Committee of East Tennessee State University and a Cottrel College Science Award of Research Corp.

References and Notes

(1) Quilico, A. Isoxazoles and Related Compounds. In *The Chemistry of Heterocyclic Compounds*; Weissberger, A., Ed.; Interscience Publishers: New York, 1962; Vol. 17.

(2) Grunanger, P.; Vita-Finzi, P. Isoxazoles. In *The Chemistry of Heterocyclic Compounds*; Vol. 49, Taylor, E. C., Ed.; Interscience Publishers: New York, 1991.

(3) Lifshitz, A.; Wohlfeiler, D. *J. Phys. Chem*. **1992**, *96*, 4505.

(4) Okada, K.; Saito, K. *J. Phys. Chem*. **1996**, *100*, 9365.

(5) Gaussian 94, Revision B.1; M. J. Frisch, G. W. Trucks, H. B. Schlegel, P. M. W. Gill, B. G. Johnson, M. A. Robb, J. R. Cheeseman, T. Keith, G. A. Petersson, J. A. Montgomery, K. Raghavachari, M. A. Al-Laham, V. G. Zakrzewski, J. V. Ortiz, J. B. Foresman, J. Cioslowski, B. B. Stefanov, A. Nanayakkara, M. Challacombe, C. Y. Peng, P. Y. Ayala, W. Chen, M. W. Wong, J. L. Andres, E. S. Replogle, R. Gomperts, R. L. Martin, D. J. Fox, J. S. Binkley, D. J. Defrees, J. Baker, J. P. Stewart, M. Head-Gordon, C. Gonzalez, and J. A. Pople; Gaussian, Inc.: Pittsburgh PA, 1995.

(6) Becke, A, D, *J. Chem. Phys.* **1993**, *98*, 5648.

(7) Lee, C.; Yang, W.; Parr, R. G. *Phys. Rev.* **1988**, *B37*, 785. Miehlich, B.; Savin, A.; Stoll, H.; Preuss, H. *Chem. Phys. Lett*. **1989**, *157*, 200.

(8) Hehre, W. J.; Ditchfield, R. D.; Pople, J. A. *J. Chem. Phys.* **1972**, *56*, 2257.

(9) Stiefvater, O. L *J. Chem. Phys*. **1975**, *63*, 2560. Stiefvater, O. L.; Nosberger, P.; Sheridan, J. *Chem. Phys*. **1975**, *9*, 435.

(10) Speroni, G.; Pino, P. *Proc. XI Int. Congr. Pure Appl. Chem. London* **1974**. Jensen, K.; Friediger, A. *Kgl. Danske Videnskab. Selskab, Mater.-Fys. Medd*. **1943**, *20*, 1.

(11) Speroni, G.; Pino, P.; Mori, L. *Gazz. Chim. Ital*. **1952**, *82*, 269.

(12) Mackrodt, W. C.; Wardleg, A.; Curnuck, P. A.; Owen, N. L.; Sheridan, J. *Chem. Commun*. **1966**, 692. Lowe, S. E.; Sheridan, J. *Chem. Phys. Lett*. **1978**, *58*, 79.

(13) Rauhut, G.; Pulay, P. *J. Phys. Chem*. **1995**, *99*, 3093.

(14) Scott, A. P.; Radom, L. *J. Phys. Chem*. **1996**, *100*, 16502.

(15) Pouchan, C.; Dargelos, A.; Chaillet, M.; Ford, G.; Katritzky, A. R. *J. Mol. Struct*. **1976**, *33*, 39. Pouchan, C.; Senez, S.; Raymond, J.; Sauvaitre, H. *J. Chem. Phys*. **1974**, *71*, 525.

(16) Pulay, P.; Torok, F. *Acta Chim. Sci. Hung*. **1965**, *47*, 273.

(17) Eyring, H. *J. Chem. Phys.* **1935**, *3*, 107. Evans, M. G.; Polanyi, M. *Trans. Faraday Soc*. **1935**, *31*, 875.